https://doi.org/10.5194/gchron-2020-36
Preprint. Discussion started: 25 November 2020

Technical note: On the reliability of laboratory beta-source calibration for luminescence dating

Barbara Mauz[1], Loïc Martin[2], Michael Discher[1], Chantal Tribolo[2], Sebastian Kreutzer[3,2], Chiara Bahl[1], Andreas Lang[1], Nobert Mercier[2]

[1] Department of Geography and Geology, University of Salzburg, 5020 Salzburg, Austria
[2] IRAMAT-CRP2A, UMR 5060, CNRS-Université Bordeaux Montaigne, 33600 Pessac, France
[3] Geography & Earth Sciences, Aberystwyth University, Aberystwyth SY23 3FL, United Kingdom

Correspondence to: Barbara Mauz (barbara.mauz@sbg.ac.at)

Abstract

The dose rate of the $^{90}Sr/^{90}Y$ beta source used in most luminescence readers is a laboratory key parameter. There is a well-established body of knowledge about parameters controlling accuracy and precision of the calibration value but some hard to explain inconsistencies still exist. Here we have investigated the impact of grain size, aliquot size and irradiation geometry on the resulting calibration value through experiments and simulations. The resulting data indicate that the dose rate of an individual beta source results from the interplay of a number of parameters, most of which are well established by previous studies. Our study provides evidence for an additionally complicating parameter which is aliquot size in particular for grain sizes of 50-200 µm. For this grain-size fraction the absorbed dose is enhanced by ~10-20% as aliquot size decreases. This enhancement is most variable for 50-100 µm grains mounted as aliquots of <8mm size and is possibly slightly reversed when large grains are mounted as small aliquots owing to the change of the geometrical function. While the build-up of charge dictates the increase of absorbed dose with the increase of grain size, this principle becomes more variable with changing irradiation geometry. We conclude that future calibration samples should encompass small, medium, large and very large grain sizes measured with small, medium and large aliquots and that each subsample should obtain several gamma doses. In this way the calibration value is obtained from the inverse slope of the fitted line, not from a single data point for all possible irradiation geometries of an individual beta source.

1 Introduction

The dose rate of the $^{90}Sr/^{90}Y$ beta source used in most luminescence readers is a laboratory key parameter. If the source's calibration is incorrect, results for equivalent dose and age are also incorrect. The significance of beta-source calibration is therefore well-known and has been subject to inter-laboratory comparison studies (e.g., Pernicka and Wagner 1979; Göksu et al., 1995).

Past studies have established that charge build-up, attenuation and backscatter constitute the physical mechanisms controlling the dose absorbed in the sample's mineral grain. The interplay of these mechanisms depends on mineral type (Aitken, 1985), on grain transparency (Bell and Mejdahl, 1981), on beta-source to grain distance (Wintle and Aitken, 1977), on grain size (Goedicke, 2007; Armitage and Bailey, 2005; Mauz and Lang, 2004)

https://doi.org/10.5194/gchron-2020-36
Preprint. Discussion started: 25 November 2020

and on the sample carrier's substrate (Greilich et al., 2008; Armitage and Bailey, 2005; Mauz and Lang, 2004; Wintle and Aitken, 1977). In addition, accuracy and/or precision of the calibration value depend on the measurement protocol (Guérin and Valladas, 2014; Kadereit and Kreutzer, 2013), on the interplay between sample and sample carrier (Hansen et al., 2018) and on the accuracy of the gamma dose to mineral calculation (Burbidge et al., 2016; Tribolo et al., 2019). Despite this well-established body of knowledge, Hansen et al. (2015) note an unexplained 3% dispersion of their calibration data, subsequently investigated by Autzen et al. (2017). They show that over-dispersed calibration data result from attenuation and backscattering, which change in response to changing grain shape and changing sample-carrier material (Autzen et al., 2017). As a consequence, the beta-dose rate should decrease for grain sizes >100 mm (Wintle and Aitken, 1977) because with increasing grain size the contribution of low-energy backscatter decreases and the primary energy spectrum is more attenuated (Hansen et al., 2018; Greilich et al., 2008). While this has improved our understanding of calibration data significantly, some details are still not fully explained. Here we test the hypothesis that, in addition to grain size and disc substrate, aliquot size and beta-source shape influence the dose rate. We carried out experiments using three quartz calibration samples characterised by three different grain-size fractions arranged in aliquots of different sizes and compared the experimental data with simulated data obtained from *GEANT4* (Agostinelli et al., 2003) and *MCNP6* (Werner, 2017; Werner et al., 2018). The results from experiments should allow identifying the impact of grain size, aliquot size and beta-source shape on the dose rate. The simulations should provide a more complete picture on the impact of individual parameters that is hard to achieve with experimental data due to experimental uncertainties being typically above 5%. We show here that grain size and aliquot size impact on the absorbed dose in response to the irradiation geometry and that this interplay should be reflected in the design of calibration measurements.

2 Experimental details

2.1 Luminescence readers and beta sources

For all experiments $^{90}Sr/^{90}Y$ beta sources with E_{max} = 2.26 MeV (Aitken, 1985) built in three different *lexsyg* luminescence readers of Freiberg Instruments were used. One is the *lexsyg RESEARCH* reader (Richter et al., 2013) equipped with a beta source arranged in a ring of 17 sealed "mini-sources" with a nominal activity of 1.51 GBq. The other two readers are *lexsyg SMART* readers (Richter et al., 2015), one is equipped with a planar beta source and the other is equipped with a ring composed of 23 "mini-sources", both with a nominal activity of 1.85 GBq. The *SMART* ring-shaped source is closed to the top (hereafter named 'closed ring') while it is open in the *RESEARCH* (hereafter named 'open ring') to allow for radio-fluorescence measurements. The beta sources in the readers were manually adjusted to align the centres of sample carrier and source in order to obtain a uniform bell-shaped irradiation field across the cup.

2.2 Calibration samples

Samples used for the experiments are listed in Table 1. The Risø fine-grain sample (batch#108) is described in Hansen et al. (2015). Tribolo et al. (2019) report on gamma irradiation and calculation of absorbed gamma dose.

https://doi.org/10.5194/gchron-2020-36
Preprint. Discussion started: 25 November 2020

Table 1. Samples and their codes used in the experiments. DTU Nutech (Denmark); SSDL: Secondary Standard Dosimetry Laboratory, Munich. For SSDL calibration samples the absorbed gamma dose and its uncertainty is derived from Monte Carlo (MC) simulation. The uncertainty of the dose (2.1%) is the quadrature of errors resulting from the MC simulation (1.4%), from the air kerma (1%) and from the geometry of the irradiation field (1.2%); see also Table 2 in Tribolo et al. (2019). For DTU calibration samples the calculation was revised (M Autzen, pers. com., Dec 2019).

Sample	Sample code	Grain size (µm)	γ-Dose (Gy)	γ-Dose Lab
Risø batch#17,	R17_180	180-250	5.0±0.1	DTU
Risø batch#113	R113_180	180-250	5.0±0.1	DTU
Risø batch#108	R108_4	4-11	5.0±0.1	DTU
Freiberg-2019	F19_90	90-160	3.00±0.06	SSDL
Freiberg-2014	F14_90	90-160	3.00±0.06	SSDL

2.3 Sample carrier

To limit the complexity of the study only one type of sample carrier was used in our experiments. The sample carrier is a cup (Fig. 1) with dimensions varying by up to 0.1 mm (our own measurements of 10 cups). The cup is made of standard stainless steel ("Stainless Steel 1.4841"; short name: X15CrNiSi25-21) with chemical composition of C (≤ 0.20 %), Si (≤ 1.5-2.5%), Mn (≤ 2.00 %), P (≤ 0.045 %), S (≤ 0.015 %), Cr (24.00 – 26.00%), Ni (19.00-22.00 %), N (≤ 0.11 %), and Fe (>50%). The material is heat resistant up to ca 1150 ˚C (e.g., https://www.thyssenkrupp-materials.co.uk/stainless-steel-314-14841.htm).

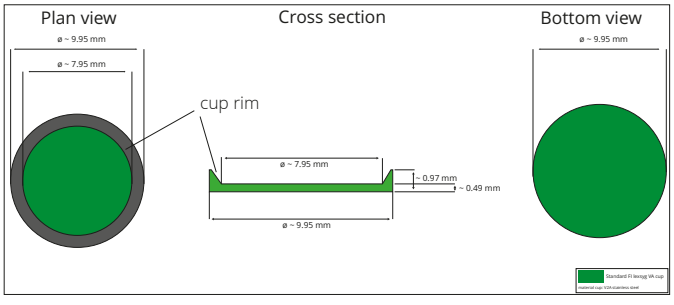

Fig. 1. The shape of the stainless-steel sample carrier (cup) used in the *lexsyg* readers.

https://doi.org/10.5194/gchron-2020-36
Preprint. Discussion started: 25 November 2020

2.2 Measurement protocol

A standard single-aliquot regenerative dose (SAR) protocol was employed with irradiation doses adjusted to encompass the expected interpolation point on the dose-response curve and test doses typically around 10% of the expected interpolation point (in seconds). The efficiency of the protocol was tested using un-dosed sub-samples (dose recovery better than 5%; Tribolo et al., 2019). The measurement parameters are listed in Table 2.

Table 2. Samples, luminescence readers and measurement parameters used in the experiments. Stimulation power was 5, 10, 70, 100 mW cm^{-2} of the blue LEDs (458±5 nm) depending on the size of the aliquot; PH/CH: preheat and cut heat temperatures for regeneration and test doses, respectively; preheat was for 10 s. For sample description see also Table 1.

Sample	Reader and beta-source geometry	Aliquot size (mm)	*n* measured	PH/CH (°C)
R17_180	*Research* open ring	8	5	260/260
		3	10	
		1	4	
F19_90	*Research* open ring	8	5	260/260
		3	5	
		1	4	
R108_4	*Research* open ring	8	10	240/200
R17_180	*SMART* planar	8	5	260/260
		3	10	
		1	4	
F19_90	*SMART* - planar	8	5	260/260
		3	5	
		1	4	
R108_4	*SMART* - planar	8	10	240/200
F14_90	*SMART* - closed ring	1	4	200/200
		5	6	
R113_180	*SMART* - closed ring	5	58	230/200
R_4	*SMART* - closed ring	8	2	240/200

3 Simulation details

The simulation of the irradiation in the *lexsyg SMART* was performed using the *GEANT4* and *MCNP6.2* toolboxes. The irradiation geometry simulated (Fig. 2) was adopted from the technical description of the manufacturer and from the sample carrier description (Fig. 1) with the sample placed in the centre of the cup. Source and housing including the fixing screws were represented as one stainless-steel cylinder surrounded by a stainless-steel shield. The quartz grains were not considered individually but represented as a cylinder the size of which was modified according to the grain size (height) and aliquot diameter to be simulated. For simulating the depth of dose rate in

https://doi.org/10.5194/gchron-2020-36
Preprint. Discussion started: 25 November 2020

a given aliquot the "sample cylinder" was sub-divided in 5 mm or 10 mm thick layers depending on the grain size to be modelled. The material was SiO_2, with a density of 1.8 g cm^{-3} which is the typical density of sand and silt composed of spherical grains. A 5 µm layer of silicon oil was added between the sample and the sample carrier for the simulation of coarse-grain aliquots (grain sizes from 25 µm to 250 µm).

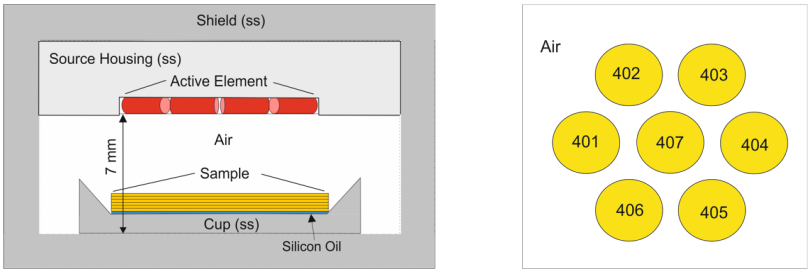

Fig.2. The geometry of the $^{90}Sr/^{90}Y$ source in the *lexsyg SMART* as designed for the simulation. Left – the *GEANT4* simulations (not to scale; ss=stainless steel). The active element is a ring of 17 small beta sources closed to the top or it is a planar foil. The cylinder-shaped sample is represented by 5-10 mm thick layers resting on a 5 mm layer of silicon oil (blue colour). The aliquot size illustrated is 7.95 mm. The distance between bottom of cup and surface of source is 7 mm; Right – pan view on individual grains represented as spheres of SiO_2 used in the *MCNP6* simulations. Cell numbers 401-406 represent 'edge grains' and cell number 407 is the central grain.

The spectra of the $^{90}Sr/^{90}Y$ beta source were simulated using the *GEANT4* radioactive decay function (Hauf et al., 2013). 10^8 disintegrations of ^{90}Sr were simulated in each run, and three runs were carried out for each aliquot configuration. The PENELOPE code for low-energy particle physics (Baró et al., 1995; Ivanchenko et al., 2011) was employed to calculate path and interaction of the beta particle with the structures presented in the model. The dose deposited in the SiO_2 target was recorded in the whole sample cylinder, and a dose-rate profile was constructed as a function of depth in the sample. For simulating small aliquots the target was split into 7 spherical cells (Fig. 2B) and the *F6 tally which is the statistical parameter in MCNP that forms the basis of absorbed dose calculations, was used to simulate the energy deposition averaged over the target cell (J/kg=Gy per starting particle) for electrons and photons separately. The output files produced by the *MCNP6* code were used to quantify photon and electron production originating from the interaction mechanisms between beta particle and matter (for details see supplement). The precision of the *GEANT4*-derived result was calculated for each aliquot configuration at the 95% confidence level (0.95 CL), based on the standard deviation between the results of the three runs per simulation. The uncertainty of the *MCNP6*-derived result was obtained from the fractional standard deviation calculated by the Monte Carlo routine.

4 Results

4.1 The calibration material

The calibration samples provided by the manufacturers show high sensitivity to dose and, consequently, excellent reproducibility as evident from the low uncertainties (Table 3). Small to large differences between samples are

https://doi.org/10.5194/gchron-2020-36
Preprint. Discussion started: 25 November 2020

evident from the experimental data which are not systematic, but seem to depend on measurement parameters (e.g., aliquot size) and, eventually, on the calculation of the gamma dose (Tribolo et al., 2019). In fact, Tribolo et al. (2019) identified an up to 14% difference of dose rate between samples when analysing single grains of the same calibration samples used here (F14_90; R113_180; Table 2). This was subsequently reduced to 5% (D Richter, pers.com, Aug 2020) when one of the manufacturers corrected their gamma dose calculation (M Autzen, pers. com., Dec 2019).

Table 3. Beta-source calibration data. Open Ring is the beta source of the *lexsyg RESEARCH* reader, planar is the one of the *lexsyg SMART* (built 2017) reader and closed ring is the one of the other *lexsyg SMART* (built 2014) reader (Fig. 1). All calibration values were first calculated from mean ± standard error (n = 4-10) and then corrected for the decay of the $^{90}Sr/^{90}Y$ source using $t_{1/2}$ = 28.79 years and the time elapsed since reference datum (21/01/2020). The uncertainty was derived from standard propagation of uncertainties of experimental and gamma-dose errors (fg = fine grain). Uncertainty of the normalised value is relative to the numerator. For details see text.

Beta source	Grain size (mm)	Aliquot size (mm)	Dose rate (Gy/s) corrected	Uncertainty (%)	Dose rate normalised to fg (%)
Open Ring	180-250	8	0.0617±0.0013	2.1	97.77±1.90
		3	0.0592±0.0012	2.1	93.57±1.97
		1	0.0633±0.0013	2.0	99.95±1.99
Open Ring	90-160	8	0.0631±0.0091	2.5	99.66±1.44
		3	0.0621±0.0015	2.5	98.19±2.40
		1	0.06411±0.0017	3.4	101.30±2.74
Open Ring	4-11	8	0.0633±0.0013	2.0	100.00±2.00
Planar	180-250	8	0.1167±0.0035	3.0	104.62±3.18
		3	0.1297±0.0027	2.1	116.24±2.43
		1	0.1247±0.0037	3.0	111.76±3.36
Planar	90-160	8	0.1184±0.0027	2.3	106.31±2.42
		3	0.1296±0.0035	2.7	116.19±3.12
		1	0.12282±0.0042	3.3	114.93±3.81
Planar	4-11	8	0.1116±0.0023	2.0	100.00±2.00
Closed Ring	180-250	8	0.1460±0.0032	2.2	102.10±2.21
		5	0.1440±0.0030	2.1	100.70±2.09
		1	0.1580±0.0036	2.3	110.49±2.49
Closed Ring	90-160	5	0.1670±0.0057	3.4	116.78±3.98
		1	0.1800±0.0052	2.9	125.87±3.60
Closed Ring	4-11	8	0.1430±0.0029	2.1	100.00±2.00

4.2 Uncertainty of data

The total uncertainty of the experimental data is 5-8% (0.95 CL). It is derived from the OSL measurement statistics, the uncertainty of the gamma dose and the quantiles of Student's *t*-distributions. For the *GEANT4*-

https://doi.org/10.5194/gchron-2020-36
Preprint. Discussion started: 25 November 2020

derived simulation data the uncertainty is 0.15-3.00% where the majority of the data show an uncertainty of <1% owing to the expected excellent reproducibility of the simulation runs. The MCNP uncertainty is the fractional standard deviation which is typically 0.1-1.1% in our study.

Table 4. Differences (%) between dose rates obtained from the 3 grain-size fractions and the 3 aliquot sizes used in the experiments. 180:90 is the difference between the two coarse-grained samples; 4:90 and 4:180 is the difference between the fine grained and the coarse-grained samples. Errors are quoted on the 95% confidence level resulting from the Student's *t*-distribution.

Grain size comparison	Aliquot size 8 mm (%)	Aliquot size 3/5 mm (%)	Aliquot size 1 mm (%)	Beta-source geometry
180:90 (μm)	0.491±0.004	4.068±0.004	1.001±0.0016	open ring
	1.579±0.007	0.075±0.006	2.512±0.012	planar
	-	15.972±0.008	13.924±0.009	closed ring
4:90 (μm)	1.281±0.004	1.912±0.003	0.653±0.003	open ring
	6.144±0.006	14.259±0.006	13.070±0.006	planar
	-	16.783±0.013	25.874±0.013	closed ring
4:180 (μm)	1.776±0.003	5.902±0.003	0.356±0.003	open ring
	4.638±0.006	14.324±0.006	10.619±0.006	planar
	2.097±0.013	0.6993±0.013	10.485±0.013	closed ring

4.3 Grain size and aliquot size

Our experimental data indicate a grain-size dependence that varies for the coarse-grained samples (90-160 μm and 180-250 μm) with aliquot size and beta-source geometry between 0% and 26% (Fig. 3, Fig. S1 and Table 4). We regard differences between individual values of >5% as informative and differences >8% as significant because the 95% t-distribution of the experimental uncertainty is 4.6 – 7.6% for the normalised dose rate values. All differences and their respective uncertainties are listed in Table 4.

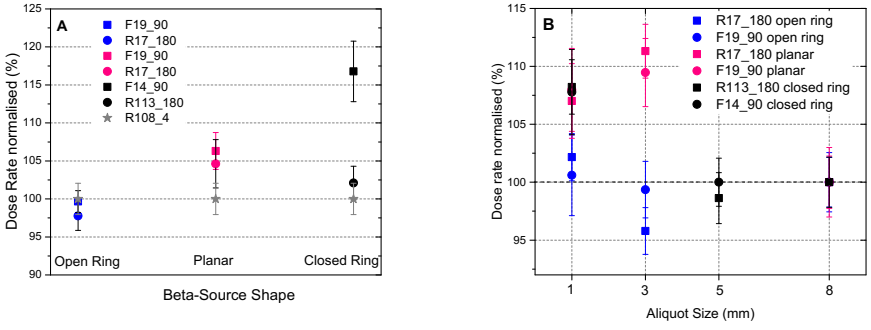

Fig. 3. Experimentally determined normalised beta-dose rates. A - dose rate normalised to the respective fg-value (sample R108_4) versus beta-source shape; Aliquot size is 8 mm. B – dose rate normalised to 8 mm aliquot size plotted versus aliquot size. For data and uncertainty see Table 3.

https://doi.org/10.5194/gchron-2020-36
Preprint. Discussion started: 25 November 2020

The experimental data indicate that the impact of grain size on the dose rates is insignificant for large (8 mm) aliquots. For aliquot sizes <8 mm the difference between the two coarse-grained samples is also negligible except for the closed-ring source. In contrast, the difference between fine-grain and coarse-grain dose rates is 6-26% and the magnitude of the difference is controlled by the shape of the source. With decreasing aliquot size, the dose rate remains constant for the smaller coarse grains (90-160 µm) and seems to decrease for large grains (180-250 µm), but this latter decrease is statistically not significant. Only with the planar source the dose rate increases by ~10% for both coarse-grain fractions (Fig. 4).

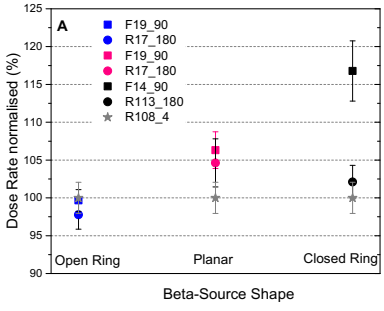

Fig. 4. Beta-dose rates of 1 mm aliquots normalised to the 8 mm aliquot size of the respective sample versus beta-source shape. For data and uncertainty see Table 3.

The data obtained from the simulations indicate a rise of dose rate with increasing grain size (Fig. 5). There is a striking similarity between the simulated data and the experimental data adopted from Armitage and Bailey (2005), but the simulation shows a gradual change of the grain-size effect, while the experiment indicates a "jump" of the dose rate in the grain-size range 50-100 µm (Fig. 5).

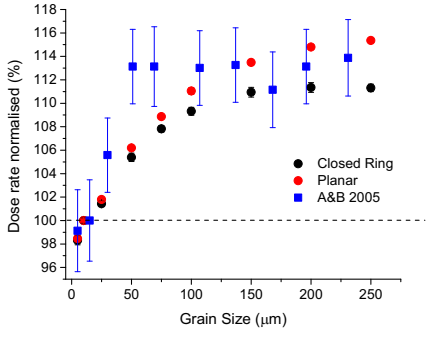

Fig. 5. Result from *GEANT4* simulation compared to published experimental data. The dose rate is plotted as a function of grain size for the planar source (black dots), for the closed-ring source (red dots) and for experimental data (A&B 2005; Armitage and Baily, 2005). Simulated data are normalised to the 10 µm

https://doi.org/10.5194/gchron-2020-36
Preprint. Discussion started: 25 November 2020

grain size, aliquot size is 7.95 mm on stainless steel cup. Experimental data of A&B 2005 are normalised to the 15 µm grain size with aliquot size of 9 mm on aluminium disc.

Because source-to-sample distance is the same in simulation and experiment, charge build-up as a function of grain size should also be the same. We discuss this in section 5. The simulations also indicate that decreasing aliquot size enhances the dose rate by ~10-20% (Fig. 6). This significant gain of absorbed dose is probably caused by the secondary electron field and is discussed in section 5.

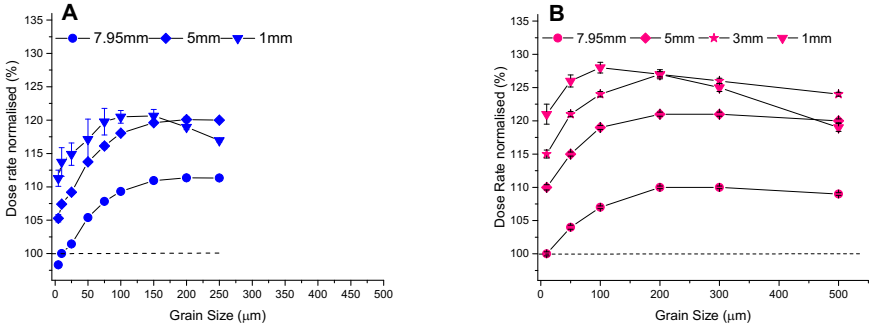

Fig 6. Result from simulations for dose rate as a function of grain size and aliquot size. Dose rate is normalised to the 10 µm grain size and 7.95 mm aliquot size expressed in percent; A – *GEANT4* for the closed-ring beta source; B – *MCNP6* for the planar beta source and grain sizes up to 500 µm to assess the significance of the trend.

4.4 Beta-source shape

There is compelling evidence from both experimental and simulation data (Figs 3, 4, 5 and 6) that the geometry of the irradiation influences the dose rate. The effect of grain- and aliquot size is the smallest for the open-ring and the biggest for the closed-ring source (Table 4). Because both sources simulated here (planar and closed ring) show the same response to aliquot size and grain size (Figs 5, 6), we conclude that the shape of the source controls the magnitude of the dose rate. This is confirmed when simulating charge build-up as a function of depth in aliquot (Fig. 7). The generalised rule seems to be correct in particular for large- and medium-sized aliquots but not for aliquot sizes < 5 mm (see details in section 4.5).

https://doi.org/10.5194/gchron-2020-36
Preprint. Discussion started: 25 November 2020

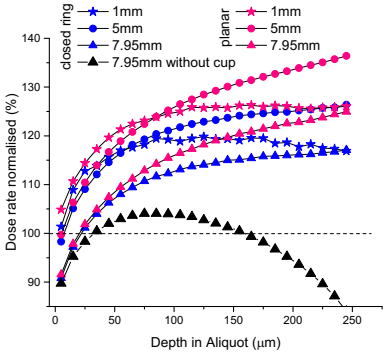

Fig. 7. Result from *GEANT4* simulation: Charge build-up in quartz grains of 250 µm size resting on a 7.95 mm ss-cup compared to no cup as a function of depth in the sample for the two beta-source geometries. The sample is composed of 10 µm thick cylinder-shaped layers (see Fig. 1). Dose rate is normalised to the 10 µm grain size and 7.95 mm aliquot size and represented in percent.

4.5 Small aliquots

A drop of dose rate for grain sizes >200 µm and aliquot sizes <5 mm is evident from the dose deposition versus depth in grain (Fig. 7), from the comparison between grain- and aliquot size (Fig. 6) and from the irradiation profile across the cup (Fig. 8). Experimental data show this drop only for the planar source, albeit indistinguishably within uncertainties.

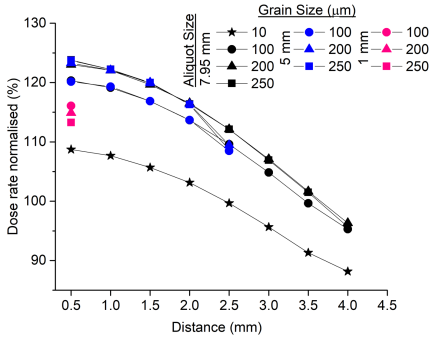

Fig. 8. Result from *GEANT4* simulation: dose rate versus distance from centre of the stainless-steel cup for the closed-ring beta source. Data are for large (7.95 mm), medium (5 mm) and small (1 mm) aliquot sizes and for 10, 100, 200, 250 µm grain sizes. Dose rate is normalised to 10 µm grain size and large aliquot.

When large grains (i.e., >200 µm) are mounted as small aliquot the ratio between surface of edge grains (see Fig. 2B for edge grain) and surface of aliquot is bigger than for small grains. The probability of beta particles interacting with these grains is approximately lineally related to the surface ratio and, thus, the bigger the surface ratio the smaller the probability of a beta particle interacting with the edge grain. In fact, the simulation shows

https://doi.org/10.5194/gchron-2020-36
Preprint. Discussion started: 25 November 2020

that the number of scattered electrons decreases for the edge grains (Fig. 9). This 'edge effect' seems to reduce the absorbed dose by ~5% (Fig. 8). However, with changing sphericity of grains (e.g., Autzen et al., 2017) and with potentially changing density of grain packing when the ideal grain monolayer is not achieved, the probability of beta interaction changes as well. Therefore, the significance of the edge effect on dose-rate calibration remains to be investigated in greater detail.

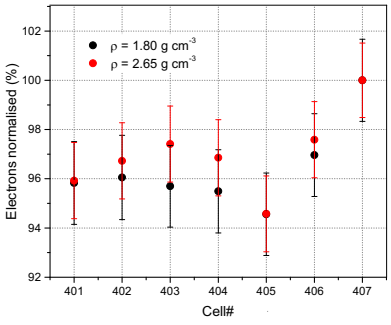

Fig. 9. Result from *MCNP6* simulation: The number of electron-producing interactions plotted against cell number. The cell is a rounded SiO_2 grain of 300 µm diameter of the two densities displayed. Data are normalised to cell#407 which is the grain surrounded by other grains (for spatial arrangement of cells see Fig. 2B).

4 Discussion

The data presented here indicate that the dose rate of an individual beta source result from the interplay of a number of parameters. Most of these were identified by previous studies including grain-size dependent build-up and attenuation of charge (e.g., Wintle and Aitken, 1977; Goedicke 2007; Autzen et al., 2017). During SAR-based measurements using a $^{90}Sr/^{90}Y$ beta source, incident beta particles penetrate the grain to a certain depth alongside back-scattered electrons which have energies less than the initial source energy (Bell, 1980). Thus, the absorbed beta dose should decrease with increasing grain size (Wintle and Aitken, 1977; Goedicke, 2007; Hansen et al., 2018). That is why Hansen et al. (2018), building on findings of Greilich et al. (2008), attribute the undesirable over-dispersion of their calibration value to variation of grain-shape and -volume because low-energy beta particles are increasingly attenuated in grains >100 µm as already described by Bell (1980). In our simulation however, charge build-up over-compensates the effects of attenuation resulting in a sustained rise of absorbed beta dose in grains >150 µm resting on material of relatively high *Z* (Fig. 8). As a consequence, the simulation shows a continued rise of dose for grains 10-300 µm (Fig. 7) with a flattening of the rise above ~150 mm grain size. This is arguably different, but not too dissimilar, to datasets deduced from experiments: Geodicke (2007) show an initial rise of dose up to 25-50 µm grain size, followed by a dose plateau for grain sizes 40-130 µm and a decrease for grains >200 µm and Armitage and Bailey (2006) show a rise to ~40 µm followed by a 'jump' to a dose plateau for 50-250 µm grains. Thus, the competing mechanisms of build-up and attenuation lead to divergent dose-rate results mainly for ~50-200 µm grains, likely caused by the geometrical function of the irradiation field (Bell, 1980).

https://doi.org/10.5194/gchron-2020-36
Preprint. Discussion started: 25 November 2020

Our study provides evidence that aliquot size is an additional parameter affecting the absorbed dose. While large aliquots show the expected build-up of charge with increasing grain size towards secondary equilibrium, the absorbed dose is larger in smaller aliquots (Figs S3-S6). This dose enhancement is not the same in simulation and experiment and is not the same for all grain sizes. The differences are caused by different penetration depths in grains and by the changing surface ratio between grains and aliquot. The interplay seems to have the most variable effect on 50-100 μm grains mounted as aliquots of <8 mm size (Fig. S8). The dose enhancement is possibly reversed when large grains (i.e., >200 μm) are mounted as small aliquots because with this geometry the probability of beta particles hitting the edge grain is reduced.

We also show that the shape of the beta source controls the magnitude of the absorbed dose, hence the build-up of charge. The fact that the dose absorbed in small grains must be lower than the dose absorbed in large grains is masked by the ring sources for which fine and coarse grains may absorb the same dose depending on the size of the aliquot (Fig. 4A).

Autzen et al. (2017) recommend minimising shape and volume variation of sample grains used for calibration, but our data suggest using multiple grain-size fractions for calibration. We think that as long as the sample originates from a natural sedimentary deposit, either way it includes grains of various shape and form. We echo Goedicke (2007) in that the calibration procedure should employ small (4-20 μm), medium (20-80 μm), large (80-200 μm) and very large (200-300 μm) grain sizes and add to this, that these grain-size fractions should be measured with small, medium and large aliquots. Thereby, calibration values are established that cover all possible irradiation geometries of an individual beta source and this, in turn, improves the calibration accuracy with respect to the unknown natural sample.

Within the limits of the SAR protocol the experimental uncertainty of the calibration value is usually reasonably low, thanks to the purpose-prepared sample material. However, with regard to beta-source calibration a higher precision is desirable. Burbidge et al. (2016) show that parallel multiple-aliquot calibration transfer provides better accuracy and precision than single-aliquot measurements on single-dosed samples. Bos et al. (2006) show that the uncertainty can be reduced to 0.9%. Their procedure envisages first, a calculation of the administered gamma dose through Fricke solutions and, second, gamma irradiating several subsamples each with a different dose (e.g., 5, 10…30 Gy) and plotting the beta D_es (s) versus the gamma doses (Gy). The inverse slope of the fitted line gives the beta-dose rate (Bos et al., 2006) and the total uncertainty is derived from the uncertainties of beta irradiation and gamma irradiation.

We can therefore say that the laboratory's key parameter can be improved in terms of accuracy and precision by including several grain sizes, several aliquot sizes and several gamma doses in the calibration experiments.

6 Conclusion

With the number of parameters in mind, it is clear that predicting the dose rate through a series of simulations is too laborious in comparison to a series of relatively simple SAR-based experiments. Here indeed additional work is required to better estimate the impact of the 'edge effect' on dose rate. If the experimental approach is the way forward, then effort should be made to improve accuracy and precision of the calibration value. Future work should therefore focus on gamma irradiating a calibration sample of several grain-size ranges with several gamma doses in order to determine the value from the regression line and not from a single data point.

https://doi.org/10.5194/gchron-2020-36
Preprint. Discussion started: 25 November 2020

Acknowledgements

We wish to thank Andreas Richter (Freiberg Instruments) for his helpful advice regarding the design of the beta sources of the *lexsyg* instruments. SK received funding from the European Union's Horizon 2020 research and innovation programme under the Marie Skłodowska-Curie grant agreement No 844457 (CREDit). He was also funded by the Conseil Regional Nouvelle Aquitaine (project DAPRES_LA_FEM).

References

Aitken, M.J., 1985. Thermoluminescence dating. Academic Press.

Agostinelli, S., Allison, J., Amako, K., Apostolakis, J., Araujo, H., Arce, P., Asai, M., Axen, D., Banerjee, S., Barrand, G., Behner, F., Bellagamba, L., Boudreau, J., Broglia, L., Brunengo, A., Burkhardt, H., Chauvie, S., Chuma, J., Chytracek, R., Cooperman, G., Cosmo, G., Degtyarenko, P., Dell'Acqua, A., Depaola, G., Dietrich, D., Enami, R., Feliciello, A., Ferguson, C., Fesefeldt, H., Folger, G., Foppiano, F., Forti, A., Garelli, S., Giani, S., Giannitrapani, R., Gibin, D., Gómez Cadenas, J.J., González, I., Gracia Abril, G., Greeniaus, G., Greiner, W., Grichine, V., Grossheim, A., Guatelli, S., Gumplinger, P., Hamatsu, R., Hashimoto, K., Hasui, H., Heikkinen, A., Howard, A., Ivanchenko, V., Johnson, A., Jones, F.W., Kallenbach, J., Kanaya, N., Kawabata, M., Kawabata, Y., Kawaguti, M., Kelner, S., Kent, P., Kimura, A., Kodama, T., Kokoulin, R., Kossov, M., Kurashige, H., Lamanna, E., Lampén, T., Lara, V., Lefebure, V., Lei, F., Liendl, M., Lockman, W., Longo, F., Magni, S., Maire, M., Medernach, E., Minamimoto, K., Mora de Freitas, P., Morita, Y., Murakami, K., Nagamatu, M., Nartallo, R., Nieminen, P., Nishimura, T., Ohtsubo, K., Okamura, M., O'Neale, S., Oohata, Y., Paech, K., Perl, J., Pfeiffer, A., Pia, M.G., Ranjard, F., Rybin, A., Sadilov, S., Di Salvo, E., Santin, G., Sasaki, T., Savvas, N., Sawada, Y., Scherer, S., Sei, S., Sirotenko, V., Smith, D., Starkov, N., Stoecker, H., Sulkimo, J., Takahata, M., Tanaka, S., Tcherniaev, E., Safai Tehrani, E., Tropeano, M., Truscott, P., Uno, H., Urban, L., Urban, P., Verderi, M., Walkden, A., Wander, W., Weber, H., Wellisch, J.P., Wenaus, T., Williams, D.C., Wright, D., Yamada, T., Yoshida, H., Zschiesche, D., 2003. Geant4—a simulation toolkit. Nuclear Instruments and Methods in Physics Research Section A: Accelerators, Spectrometers, Detectors and Associated Equipment 506, 250–303. doi:10.1016/S0168-9002(03)01368-8

Armitage, S.J., Bailey, R.M., 2005. The measured dependence of laboratory beta dose rates on sample grain size. Radiation Measurements 39, 123–127. doi:10.1016/j.radmeas.2004.06.008.

Autzen, M., Guerin, G., Murray, A.S., Thomsen, K.J., Buylaert, J-P., Jain, M., 2017. The effect of backscattering on the beta dose absorbed by individual quartz grains. Radiation Measurements 106, 491–497.10.1016/j.radmeas.2017.05.004.

Baró, J., Sempau, J., Fernández-Varea, J.M., Salvat, M., 1995. "PENELOPE": an algorithm for Monte Carlo simulation of the penetration and energy loss of electrons and positrons in matter. Nuclear Instruments Methods in Physics Research B 100 : 31-46.

Bell, W.T., 1980. Beta source calibration: Some problems associated with the utilisation of the gamma irradiation of quartz and other phosphors. Part I, Ancient TL 10, 3-9; Part II, Ancient TL 11, 2-6.

Bell, W.T., Mejdahl, V., 1981. Beta Source Calibration and Its Dependency on Grain Transparency. Archaeometry 23, 231–240. doi:10.1111/j.1475-4754.1981.tb00310.x

https://doi.org/10.5194/gchron-2020-36
Preprint. Discussion started: 25 November 2020

Bos, A.J.J., Wallinga, J., Johns, C., Abellon, R.D., Brouwer, J.C., Schaart, D.R., Murray, A.S., 2006. Accurate calibration of a laboratory beta particle dose rate for dating purposes. Radiation Measurements 41, 1020–1025. doi:10.1016/j.radmeas.2006.04.003.

Burbidge, C.I., Cardoso, J., Cardoso, G.O., Franco, J., Santos, L., Caldeira, M., 2016. Parallel calibration transfer and systematic effects in retrospective absorbed dose estimation using OSL 34, 92–101. doi:10.1016/j.quageo.2016.04.001

Goedicke, C. 2007. Calibration of a 90Sr/90Y-source for luminescence dating using OSLRadiation Measurements 42, 1427–1431. doi:10.1016/j.radmeas.2007.09.014.

Göksu, H.Y., Bailiff, I.K., Bøtter-Jensen, L., Brodski, L., Hütt, G., Stoneham, D., 1995. Interlaboratory beta source calibration using TL and OSL on natural quartz. Radiation Measurements 24, 479–483. doi:10.1016/1350-4487(95)00258-G.

Greilich, S., Murray, A.S., Bøtter-Jensen, L., 2008. Simulation of electron transport during beta irradiation. Radiation Measurements 43, 748 – 751. doi:10.1016/j.radmeas.2008.01.017.

Guérin, G., Valladas, H., 2014. Cross-calibration between beta and gamma sources using quartz OSL: Consequences of the use of the SAR protocol in optical dating. Radiation Measurements 68, 31–37. doi:10.1016/j.radmeas.2014.06.010.

Hansen, V., Murray, A., Buylaert, J.-P., Yeo, E.-Y., Thomsen, K., 2015. A new irradiated quartz for beta source calibration. Radiation Measurements 81, 123–127. doi:10.1016/j.radmeas.2015.02.017.

Hansen, V., Murray, A., Thomsen, K., Jain, M., Autzen, M., Buylaert, J.-P., 2018. Towards the origins of over-dispersion in beta source calibration. Radiation Measurements 1–6. doi:10.1016/j.radmeas.2018.05.014.

Hauf, S., Kuster, M., Batic, M., Bell, Z. W., Hoffmann, D.H.H., Lang, P.M., Neff, S., Pia, M.G., Weidenspointner, G., Zoglauer, A., 2013. Radioactive Decays in Geant4. IEEE Transactions on Nuclear Science, vol. 60, no. 4, pp. 2966-2983, Aug. 2013, doi: 10.1109/TNS.2013.2270894.

Ivanchenko, V., Apostolakis, J., Bagulya, A., Abdelouahed, H.B., Black, R., Bogdanov, A., Burkhard, H., Chauvie, S., Cirrone, P., Cuttone, G., Depaola, G., Di Rosa, F., Elles, S., Francis, Z., Grichine, V., Gumplinger, P., Gueye, P., Incerti, S., Ivanchenko, A., Jacquemier, J., Lechner, A., Longo, F., Kadr, O., Karakatsanis, N., Karamitros, M., Kokoulin, R., Kurashige, H., Maire, M., Mantero, A., Mascialino, B., Moscicki, J., Pandola, L., Perl, J., Petrovic, I., Ristic-Fira, A., Romano, F., Russo, G., Santin, G., Schaelicke, A., Toshito, T., Tran, H., Urban, L., Yamashit, T., Zacharatou, C., 2011. Recent improvements in Geant4 electromagnetic physics models and interfaces. Progress in Nuclear Science and Technology 2, 898-903.

Kadereit, A., Kreutzer, S., 2013. Risø calibration quartz – a challenge for β-source calibration. An applied study with relevance for luminescence dating. Measurement 46, 2238–2250. doi:10.1016/j.measurement.2013.03.005.

Mauz, B., Lang, A. 2004. The dose rate of beta sources for optical dating applications: A comparison between fine silt and fine sand quartz. Ancient TL 22, 45-48.

Pernicka, E., Wagner, G.A., 1979. Primary and interlaboratory calibration of beta sources using quartz as thermoluminescent phosphor. Ancient TL 2–6.

https://doi.org/10.5194/gchron-2020-36
Preprint. Discussion started: 25 November 2020

Richter, D., Richter, A., Dornich, K., 2015. Lexsyg smart — a luminescence detection system for dosimetry, material research and dating application. Geochronometria 42, 202–209. doi:10.1515/geochr-2015-0022

Richter, D., Richter, A., Dornich, K., 2013. Lexsyg — a new system for luminescence research. Geochronometria 40, 220–228. doi:10.2478/s13386-013-0110-0

Tribolo, C., Kreutzer, S., Mercier, N., 2019. How reliable are our beta-source calibrations? Ancient TL 37, 1–10.

Werner, C.J., J.S. Bull, C.J. Solomon, F.B., Brown, G.W. McKinney, M.E. Rising, D.A. Dixon, R.L. Martz, H.G. Hughes, L.J. Cox, A. J. Zukaitis, J.C. Armstrong, R. A. Forster, L. Casswell., 2018. MCNP6.2 Release Notes. LA-UR-18-20808. https://permalink.lanl.gov/object/tr?what=info:lanl-repo/lareport/LA-UR-18-20808.

Werner, C.J., 2017. MCNP Users Manual - Code Version 6.2, LA-UR-17-29981.

Wintle, A.G., Aitken, M.J., 1977. Absorbed Dose from a Beta Source as Shown by Thermoluminescence Dosimetry. International Journal of Applied Radiation and Isotopes 28, 625–628.